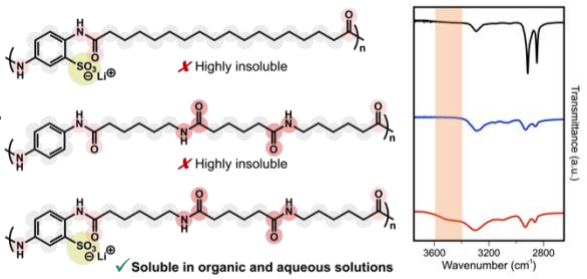
# Structural Effects on Solubility and Crystallinity in Polyamide Ionomers

Jou-Tsen Ou, Margaret K. Brown, Jason D. Kaff, Rhys W. Hughes, Dale L. Huber, Brent S. Sumerlin, Karen I. Winey, 5 and Mercedes K. Taylor \*\*

KEYWORDS precise polymer, ionomer, polyamide, processability, and solubility

**ABSTRACT:** Although polyamides have been an industrial staple for decades, their solubility and processability remain limited due to the strong hydrogen bonding between amide groups. Here, we report a new family of polyamides in which aryl rings, alkyl spacers, sulfonate groups, and amide linkages are regularly spaced along the polymer backbone, allowing us to probe the structural elements that affect processability. We accessed these polymers through a synthetic route based on an expanded diamine monomer and characterized them through a range of physical and spectroscopic techniques. Our results show that the combination of sulfonate groups with increased amide content results in highly soluble



polymers, which can dissolve in polar solvents such as water, methanol, and *N*,*N*-dimethylformamide. Infrared spectroscopy on the solid polymers shows that the aliphatic amides engage in hydrogen bonding with the sulfonate groups, thus inhibiting ion aggregation, crystallization, and microphase separation. These findings expand the avenue to sulfonate-containing polyamide chemistry and provide design rules for the synthesis of more processable ionic polyamides.

#### Introduction

Since polyamides were discovered in the 1940s, they have become ubiquitous in everyday life because of their excellent chemical resistance and mechanical strength. For example, Nylon-6,6, a representative polyamide, has been an important industrial material for textiles, automobiles, sports equipment, and furniture. The crystallinity of polyamides is vital to their mechanical properties. This crystallinity arises from hydrogen bonding among amide groups in conjunction with alkylchain stacking (in aliphatic polyamides like Nylon-6,6)7,8 or  $\pi$ - $\pi$  stacking (in aromatic polyamides like Kevlar). However, the crystallinity and high melting temperature of industrial polyamides inhibits their processability and imposes synthetic restrictions related to these polymers' very low solubilities. It is thus desirable to improve the

solubility and processability of polyamides by tuning their chemical structures.

Recent advances in polymer synthesis make it possible to design linear polymers with functional groups that repeat with an exact and known spacing along the polymer backbone. 12,13 This synthetic precision provides a high level of control over a polymer's structure, allowing better control over the resulting polymer properties. 14 Specifically, ion-containing multiblock copolymers with strictly alternating polar and nonpolar blocks have been synthesized and studied for applications in ion transport. 14-18 The structural regularity of these polymers gives rise to highly ordered ion-transport pathways, making them promising polymer electrolytes.

To endow these structurally regular "ionomers" with the mechanical advantages of polyamides, we recently reported a series of strictly alternating polyamide sulfonates in which

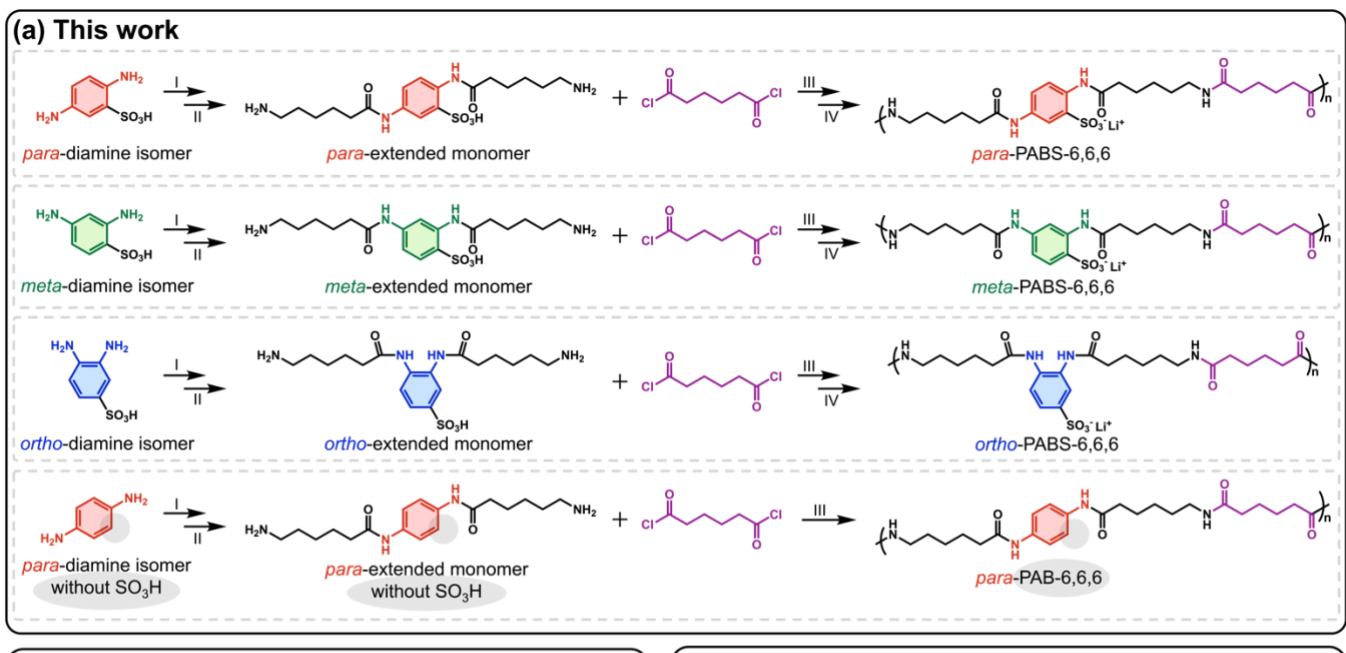
<sup>&</sup>lt;sup>1</sup>Department of Chemistry and Biochemistry, University of Maryland, College Park, MD 20742, USA.

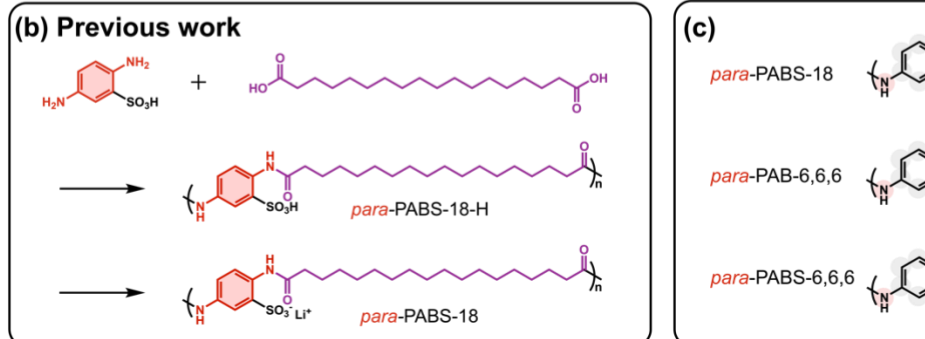
<sup>&</sup>lt;sup>2</sup>Department of Materials Science and Engineering, University of Pennsylvania, Philadelphia, Pennsylvania 19104, USA.

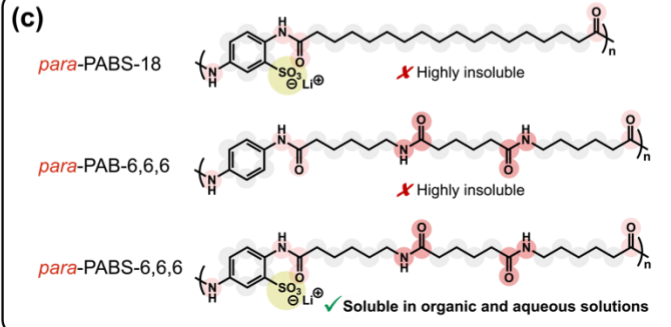
<sup>&</sup>lt;sup>3</sup>George & Josephine Butler Polymer Research Laboratory, Center for Macromolecular Science & Engineering, Department of Chemistry, University of Florida, Gainesville, Florida 32611, USA.

<sup>&</sup>lt;sup>4</sup>Center for Integrated Nanotechnologies, Sandia National Laboratories, Albuquerque, New Mexico 87185, USA.

<sup>&</sup>lt;sup>5</sup>Chemical and Biomolecular Engineering, University of Pennsylvania, Philadelphia, Pennsylvania 19104, USA.







Scheme 1. (a) This work: The synthetic route to three PABS-6,6,6 ionomers and a PAB-6,6,6 polymer from different diamine isomers. (I) Z-6-aminohexanoic acid, ethyl chloroformate, triethylamine, Hünig's base, anhydrous dichloromethane (DCM), anhydrous *N*,*N*-dimethylformamide (DMF), room temperature (rt); (II) 33% HBr in acetic acid, trifluoroacetic acid, rt; (III) adipoyl chloride, Hünig's base, anhydrous DMF, 50 °C; (IV) Lithium-ion exchange, rt. (b) Previous work: the synthesis of a strictly alternating ion-containing polyamide was performed from the melt state for *para*-PABS-18. (c) The comparison between *para*-PABS-18, *para*-PAB-6,6,6, and *para*-PABS-6,6.6.

a polar benzenesulfonate block alternates with a nonpolar hydrocarbon block.<sup>19</sup> In that work, the ionomer with the longest hydrocarbon block (number of carbons = 18, *para*-PABS-18) formed well-defined nanoscale layers. However, the poor solubility and processability of this polymer highlighted the problems with polyamides discussed above. Thus, we sought to develop a route toward new polyamide ionomers with improved processability.

To this end, we designed a series of polyamide ionomers in which the balance of aryl rings, alkyl spacers, and amide linkages affords greater control over properties related to processability (**Scheme 1**). The length of the ring-based monomer was first elongated by amide formation to yield extended monomers (**Scheme 1a**), which can be contrasted with the smaller diaminobenzene monomers used in previous work (**Scheme 1b**). The extended monomers were then polymerized to give three regioisomeric ionomers and one non-ionic polymer. Structural differences among the

new polyamides were studied across a range of length scales using infrared (IR) spectroscopy, X-ray scattering, and scanning electron microscopy. The results show that the interaction between amide linkages and sulfonate groups disrupts crystallinity and improves processability in polyamide ionomers, highlighting the importance of synthetic control over amide content and spacing. This work provides design rules for more processable and functional polyamides and expands the structural diversity of precise ionomers.

# Results and discussion

**Polymer synthesis.** The new family of polyamides was designed to meet several chemical requirements. First, sulfonate groups were periodically spaced along the polymer backbone since the sulfonate moiety is well-known to improve aqueous solubility and is of interest for ion-transport applications.<sup>20–22</sup> The sulfonate groups were placed on aryl rings to allow access to diverse regioisomers

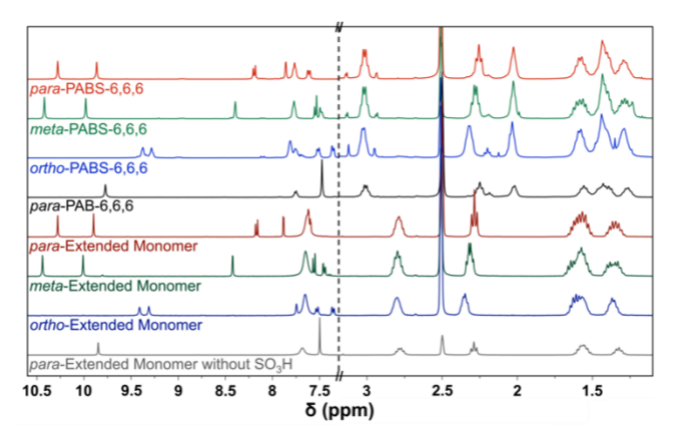


**Figure 1.** <sup>1</sup>H NMR spectra of *para-*, *meta-*, and *ortho-*PABS-6,6,6, *para-*PAB-6,6,6, *para-*, *meta-*, and *ortho-*extended monomers, and the *para-*extended monomer without SO<sub>3</sub>H.

depending on the arrangement of the polymerizable amino groups around the ring (ortho vs. meta vs. para). Next, we inserted alkyl chains between the benzenesulfonate ring and the polymerizable amino groups. In contrast to the diaminobenzene monomers we reported previously, 19 the greater distance of the polymerizable amines from the strongly electron-withdrawing benzenesulfonate groups enhances the nucleophilicity of the amines. Finally, by polymerizing these extended diamines with adipoyl chloride, we obtained polymers with a long alkyl spacer between polar benzenesulfonate groups, punctuated by amide bonds. This alkyl spacer is analogous to the 18carbon spacer we studied previously, but it contains additional amide character regularly interspersed throughout (Scheme 1c). We named the polymers according to the orientation of the amino groups on the benzenesulfonate (ortho, meta, or para), followed by either polyamide benzene (PAB) or polyamide benzenesulfonate (PABS) and the number of carbons between each amide linkage in the spacer (6, 6, 6), in homage to the Nylon-6,6 nomenclature.

First, the extended monomers were synthesized through amide formation followed by amine deprotection, and the corresponding polymers were then synthesized via stepgrowth polymerization, as shown in Scheme 1. Their chemical structures were confirmed by <sup>1</sup>H NMR, <sup>13</sup>C NMR, and ESI mass spectrometry (Figures S1-S26). Take para-PABS-6,6,6 as an example; each equivalent of *para*-diamine isomer first formed two amide bonds by reacting with two equivalents of benzyl carbamate (Cbz)-protected aminohexanoic acid, yielding a Cbz-protected paraextended monomer. A deprotection with HBr removed the CBz protecting groups on the protected para-extended monomer. The para-extended monomer has six carbons connected to each amide bond and has amino groups as end groups, allowing the para-extended monomer to be polymerized by reacting with adipoyl chloride. The polymerization was thus performed by combining the paraextended monomer with adipoyl chloride in N,Ndimethylformamide (DMF) with Hünig's base at 50 °C for three days. The product, para-PABS-6,6,6, was first purified

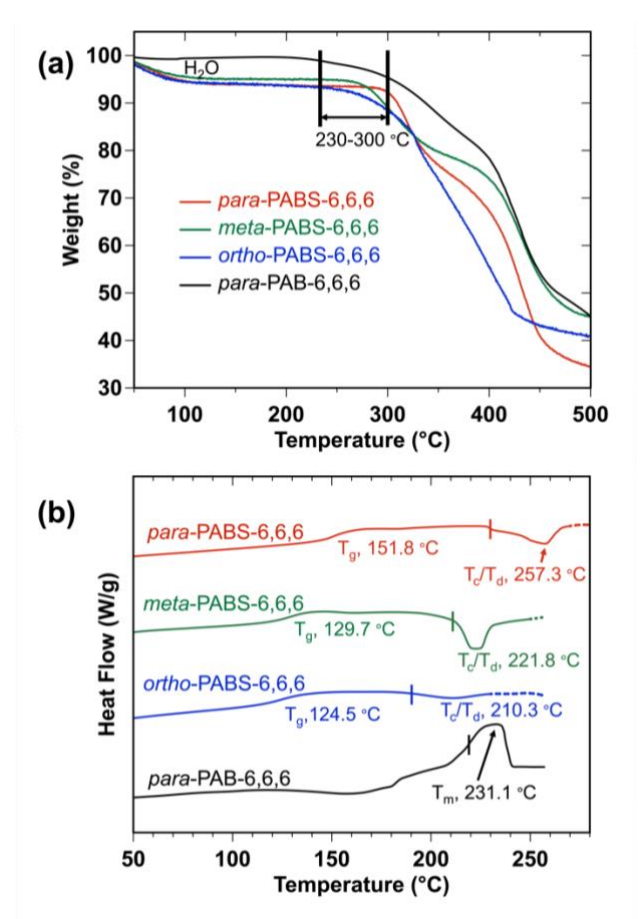


**Figure 2. (a)** TGA curves of three polyamide PABS-6,6,6 ionomers and the PAB-6,6,6 polymer in air (heating rate: 10 °C/min. **(b)** The DSC heating traces (exothermal down) of three polyamide PABS-6,6,6 ionomers and the PAB-6,6,6 polymer after annealing (heating rate: 10 °C/min; vertical lines indicate the annealing temperature for each sample; dashed curves indicate the DSC data collected after the degradation temperatures).

by aqueous dialysis to remove DMF and chloride ions. The diisopropylethylammonium counterion of the sulfonate group was then replaced with Li<sup>+</sup> by conducting a series of lithium-ion exchanges. Finally, excess lithium ions were eliminated by aqueous dialysis. Further expansion of this monomer/polyamide library was completed, which yielded three PABS-6,6,6 ionomers and the non-ionic *para-PAB-6,6,6* polymer (**Scheme 1**).

**Figure 1** shows the <sup>1</sup>H NMR spectra of the extended monomers and corresponding polymers, demonstrating that they were successfully synthesized. Because of the electron-withdrawing effect of the benzenesulfonate groups on the regioisomeric monomers and PABS-6,6,6 ionomers, the chemical shifts of amide peaks at 9.0-10.5 ppm and aromatic peaks at 6.5-8.5 ppm depend on the amide and aromatic hydrogens' positions relative to the sulfonate position. On the contrary, the aliphatic peaks and a broad amine peak at 7.67 ppm have similar positions for all three monomers, indicating that the electron-

withdrawing effect does not meaningfully influence their chemical shift. Thus, the sulfonate group does not attenuate the nucleophilicity of the aliphatic amines. After the polymerization, the broad amine peaks of the monomers at 7.67 ppm disappear, while new amide peaks of ionomers at 7.77 ppm appear, indicating that the amines are fully converted to amides. Also, after the polymerization, the  $\alpha$ -carbon next to the amine shifts downfield from 2.79 ppm in the monomers to 3.02 ppm in the ionomers. In addition, the formation of the amides leads to new broad peaks at 2.03 ppm (the  $\alpha$ -carbon of the amide). These results indicate that three extended monomers were successfully converted to the PABS-6,66 ionomers.

On the other hand, because *para*-PAB-6,6,6 does not have a sulfonate group, there is only one amide peak at 9.84 ppm, one broad amine peak at 7.67 ppm, and one aromatic peak at 7.50 ppm. After the polymerization, the broad amine peak disappears, while an amide peak appears at 7.75 ppm, confirming that the non-ionic *para*-monomer was also converted into *para*-PAB-6,6,6.

All three ionomers were soluble in water and in polar organic solvents (DMF and dimethyl sulfoxide), even after Li+ exchange. This represents a major improvement over the highly insoluble para-PABS-18, which has a similar chemical structure to para-PABS-6,6,6 but lacks the amide linkages in the 18-carbon spacer. Consequently, we conclude that the additional amide content plays a vital role in the improved solubility of the ionomers. Further, the nonsulfonated para-PAB-6,6,6 was insoluble in water and poorly soluble in the polymerization solvent (DMF), indicating that both amide content and sulfonate groups are necessary for solubility. All the sulfonate-containing polymers are brittle when dry, making solid-state processing impractical, but the enhanced solubility of the PABS-6,6,6 materials opens the door to convenient solution-state processing.

The size-exclusion chromatography (SEC) results in **Table S1** and **Figure S27** show that the molecular weights of *para-*, *meta-*, and *ortho-*PABS-6,6,6 range from 12,200–16,400 g/mol. In comparison, the molecular weight of the non-sulfonated *para-*PAB-6,6,6 polymer was found to be significantly lower (6,810 g/mol). This lower molecular weight is likely related to the low solubility of *para-*PAB-6,6,6 in DMF, inhibiting the formation of higher molecular weight polymers. (Performing the polymerization in other solvents is not feasible, as the solubility of the monomers and resulting polymer is even worse in all other solvents tested, both more and less polar.) In other words, the solubility results discussed above have implications for molecular weight as well as for processability, highlighting the importance of the current work.

**Thermal properties.** Thermogravimetric analysis (TGA) and differential scanning calorimetry (DSC) were performed to characterize the thermal properties of the PABS-6,6,6 ionomers and the PAB-6,6,6 polymer (**Figure 2**). The TGA curves (**Figure 2a**) show that the three ionomers lose water from 100 to 93-95 °C, while the non-sulfonated polymer does not show significant water loss, potentially

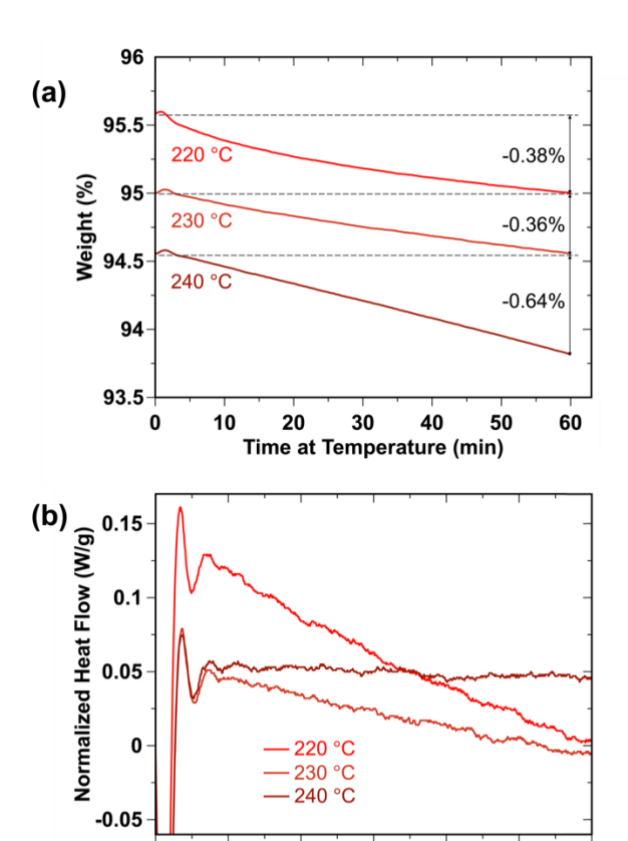


**Figure 3. (a)** TGA curves and **(b)** DSC curves (exothermal down) from isothermal simultaneous TGA-DSC experiments at three temperatures for *para*-PABS-6,6,6 under N<sub>2</sub>.

30

Time at Temperature (min)

40

60

20

0

indicating that the sulfonate group binds water. Also, the TGA curves show that the onset of mass loss of para-, meta-, and ortho-PABS-6,6,6, and para-PAB-6,6,6 are 270, 250, 230, and 300 °C, respectively, which set the temperature ranges of the DSC experiments. Based on the TGA results, we annealed para-, meta-, and ortho-PABS-6,6,6 and para-PAB-6,6,6 under inert conditions for 2 hours at 230, 210, 190, and 220 °C, respectively, before running the DSC experiments. In the DSC heating curves obtained after annealing (Figure 2b), we observed the glass transition temperatures (Tgs) of para-, meta-, and ortho-PABS-6,6,6 to be 151.8, 129.7, and 124.5 °C, respectively. We observed para-PAB-6,6,6 to show a melting (endothermic) peak at 231.1 °C, while para-, meta-, and ortho-PABS-6,6,6 exhibit broad exothermic peaks at 257.3, 221.8, and 210.3 °C, respectively, which we attribute to the onset of crystallization.

Since the crystallization temperatures are close to the degradation temperatures of PABS-6,6,6 ionomers, simultaneous TGA-DSC experiments were conducted to determine the proper annealing processes to prepare crystalline polymers for further characterization. Take *para*-PABS-6,6,6 as an example (**Figure 3**); in the TGA-DSC

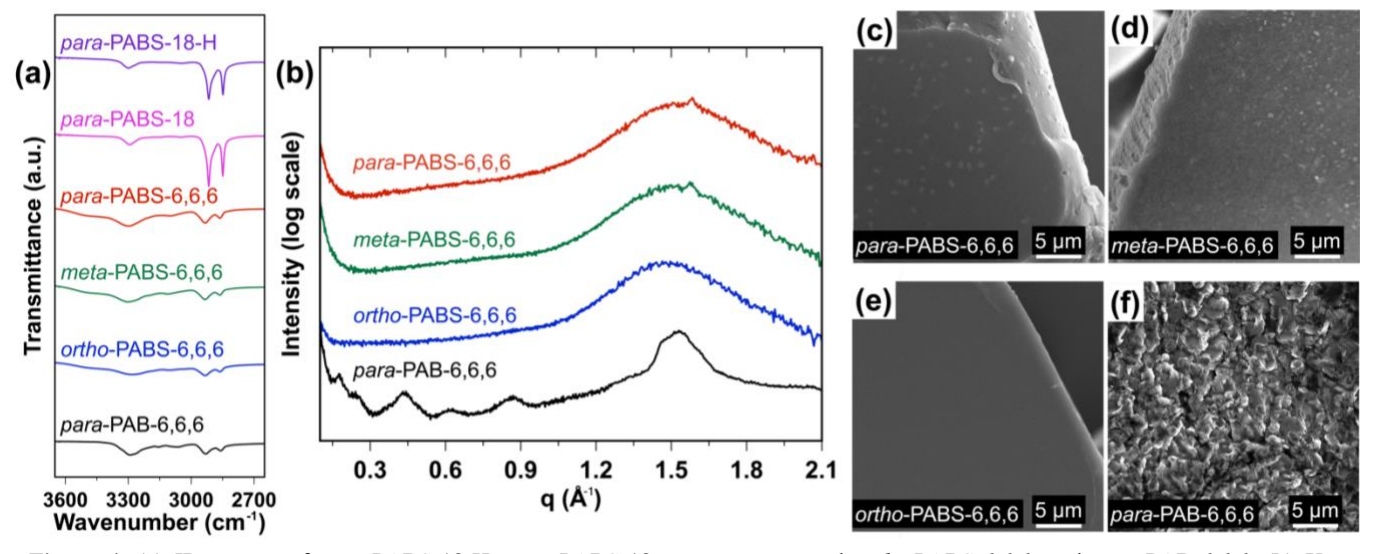


**Figure 4. (a)** IR spectra of *para*-PABS-18-H, *para*-PABS-18, *para*-, *meta*-, and *ortho*-PABS-6,6,6, and *para*-PAB-6,6,6. **(b)** X-ray scattering data for three PABS-6,6,6 ionomers and the PAB-6,6,6 polymer. SEM images of annealed **(c)** *para*-, **(d)** *meta*-, **(e)** *ortho*-PABS-6,6,6, and **(f)** *para*-PAB-6,6,6.

coupled instrument, the sample pan was heated to 220 °C at 10 °C/min and then maintained at 220 °C for 1 hour. The pan was then sequentially heated in 10 °C intervals and maintained at each temperature for 1 hour until the rate of mass loss became significant. At 220 °C, the weight loss of para-PABS-6,6,6 was only 0.38%, while the DSC curve showed that para-PABS-6,6,6 underwent an exothermic process. At 230 °C, the weight loss was only 0.36%, while para-PABS-6.6.6 underwent an exothermic process. At 240 °C, the weight loss increased to 0.64%, and the heat flow stabilized. From these results, we established a thermal history to maximize crystallization for para-PABS-6,6,6 by heating at 230 °C. This procedure allows us to anneal at the highest possible temperature without degrading the ionomer. The same methodology was applied to meta-PABS-6,6,6, ortho-PABS-6,6,6, and para-PAB-6,6,6 (Figures S28-S30), and their maximum annealing temperatures were determined to be 210 °C, 190 °C, and 220-240 °C, respectively, confirming the annealing conditions used for Figure 2b. Prior to solid state characterizations, the polymers were annealed at these temperatures for several hours.

Characterization in the solid state. IR spectroscopy, X-ray scattering, and scanning electron microscopy (SEM) were used to study the chemical environments, crystallinity, and morphologies of the annealed materials in the solid state. The IR spectra from 2650 to 3750 cm<sup>-1</sup> (Figure 4a) are informative in highlighting the chemical differences between the polymers. (Complete IR spectra from 450 to 4000 cm<sup>-1</sup> are available in Figure S31). The two bands at 2930 and 2860 cm<sup>-1</sup>, attributed to the C–H asymmetric and symmetric stretching, are present in all spectra. However, the two bands in the *para-*, *meta-*, *ortho-*PABS-6,6,6, and *para-*PABS-18 and *para-*PABS-18-H (Scheme 1b), which is attributed to the introduction of aliphatic amides into the

polymer backbones. The region between 3200-3600 cm<sup>-1</sup> is associated with N–H stretching vibrations, which are sensitive to hydrogen bonding. The N–H band appears as a relatively sharp peak at ca. 3300 cm<sup>-1</sup> for *para*-PAB-6,6,6, *para*-PABS-18, and *para*-PABS-18-H. In *para*-, *meta*-, and *ortho*-PABS-6,6,6 ionomers, the band broadens, and a shoulder emerges at 3200 cm<sup>-1</sup>. Both changes indicate that the amide N–H forms hydrogen bonds with sulfonate groups in the three PABS-6,6,6 ionomers, unlike in the *para*-PAB-6,6,6 and *para*-PABS-18, in which the amide N–H coordinates to amide carbonyls.<sup>23-25</sup>

In **Figure 4b**, the X-ray scattering patterns show that each of the annealed PABS-6,6,6 ionomers exhibit low or no crystallinity and do not self-assemble. Each PABS-6,6,6 has an amorphous halo centered around  $\sim 1.5 \ \text{Å}^{-1}$ , with a small peak observed at q = 1.58 Å-1 in *para*- and *meta*-PABS-6,6,6 corresponding to a d-spacing of 3.98 Å. These small peaks in the X-ray scattering data for *para*- and *meta*-PABS-6,6,6 correspond to the exothermic peaks at 257.3 and 221.8 °C in the respective DSC curves (see further discussion in **Figure S32**). *Ortho*-PABS-6,6,6 is entirely amorphous, which agrees with the relatively shallow peak seen in DSC. None of the PABS-6,6,6 ionomers show a feature at small angles, indicating that no microphase separation occurs.

On the other hand, the non-sulfonated *para*-PAB-6,6,6 shows overlapping peaks indicating coexisting  $\alpha$ -form and  $\gamma$ -form polyamide crystals centered about 1.52 Å-1,26 In the *para*-PAB-6,6,6 pattern, peaks at lower q indicate layered morphologies with two coexisting layer spacings of 34 Å and 29 Å (**Figure S33**). These spacings were determined by fitting the background-subtracted pattern to a summation of Gaussian curves, which are summarized in **Table S2**. In previous work, 3-layer spacings were observed in *para*-PABS-18, and these were attributed to the entire layer spacing, the distance between amide groups through the

hydrocarbon layer, and the distance between amide groups through the ionic layer. In *para*-PAB-6,6,6, the spacings of the two layers are similarly attributed to the entire layer spacing and the spacing between opposite polyamide groups within a layer. These X-ray scattering results show that for the materials studied, crystallization and self-assembly are suppressed in materials that also show the broadening and emergence of a shoulder in the N-H stretching band in IR.

**Figure 4c-f** displays SEM images of the annealed samples. In **Figure 4c-e**, the surfaces of the annealed PABS-6,6,6 ionomers are smooth, as expected for amorphous polymers annealed above their glass transition temperatures. In **Figure 4f**, the annealed *para*-PAB-6,6,6 shows structural heterogeneity on the  $\sim$ 1 µm length scale, as expected for a semi-crystalline polymer powder annealed below its melting temperature.

The differences in morphologies and structures between the PABS-6,6,6 ionomers and the para-PAB-6,6,6 polymer are explained by the favorable interactions between amides and sulfonate groups. Because aliphatic amide N-H groups hydrogen bond to SO<sub>3</sub> moieties, the interaction prevents crystallization and the self-assembly of the SO<sub>3</sub>Li groups. The aliphatic amide groups in PABS-6,6,6 ionomers, instead of forming inter-amide hydrogen bonds and crystalizing into secondary β-pleated sheet structures, engage in hydrogen bonding with the sulfonate groups, preventing microphase separation. These interactions have been reported previously and used to increase miscibility in blends of lithium-sulfonate-functionalized polystyrene and various nylons.<sup>23–25</sup> Thus, the three PABS-6,6,6 ionomers are mostly or entirely amorphous, while the para-PAB-6,6,6 polymer and para-PABS-18, with the same number of backbone carbon atoms in the monomeric unit, are crystalline. Our results emphasize that the interactions between aliphatic amides and sulfonate groups play an essential role in determining crystallization behavior in sulfonate-containing polyamides.

The physical properties of the new polyamides indicate a trade-off between long-range order and processability. We found that adding amide linkages at regular intervals through a long carbon spacer greatly improves solubility, including in water, thus enabling solution processing of these ionomers. The reduction in crystallinity and concomitant improvements in processability are driven by interactions between amide N–H groups and sulfonate groups, as shown by IR spectroscopy. This set of structure-property relationships can guide chemists in designing the next generation of processable polyamide ionomers.

## **Conclusions**

We designed a new family of polyamides that we synthesized through a route based on extended diamine monomers. The resulting polymers contain a balance of functionality (alkyl, aryl, ionic) in strictly repeating sequences, punctuated by amide linkages. We found that combining sulfonate groups with increased amide content led to improvements in processability, particularly higher solubility. These improvements were accompanied by a

decrease in crystallinity, underscoring the trade-offs inherent to the design of a processable, ordered polyamide ionomer. Infrared spectroscopy shows that hydrogen bonding between amide N-H groups and sulfonate groups drives the differences in solubility and crystallinity observed across the series of polymers. This work expands the structural diversity of polyamides and can inform the design of processable ionomers.

## ASSOCIATED CONTENT

**Supporting Information**. The Supporting Information is available free of charge via the Internet at http://pubs.acs.org. General procedures, synthetic procedures, and supplementary figures, including <sup>1</sup>H NMR, <sup>13</sup>C NMR, ESI-Mass, SEC, and IR spectra, and simultaneous isothermal TGA-DSC, X-ray scattering data.

# **AUTHOR INFORMATION**

# Corresponding Author

Mercedes K. Taylor – Department of Chemistry and Biochemistry, University of Maryland, College Park, Maryland 20742, United States. Email: mkt@umd.edu.

## Authors

**Jou-Tsen Ou** – Department of Chemistry and Biochemistry, University of Maryland, College Park, Maryland 20742, United States

**Margaret K. Brown** – Department of Materials Science and Engineering, University of Pennsylvania, Philadelphia, Pennsylvania 19104, United States.

**Jason D. Kaff** – Department of Chemistry and Biochemistry, University of Maryland, College Park, Maryland 20742, United States.

Rhys W. Hughes – George & Josephine Butler Polymer Research Laboratory, Center for Macromolecular Science & Engineering, Department of Chemistry, University of Florida, Gainesville, Florida 32611, United States.

**Dale L. Huber** – Center for Integrated Nanotechnologies, Sandia National Laboratories, Albuquerque, New Mexico 87185, United States

**Brent S. Sumerlin** – George & Josephine Butler Polymer Research Laboratory, Center for Macromolecular Science & Engineering, Department of Chemistry, University of Florida, Gainesville, Florida 32611, United States.

**Karen I. Winey** – Department of Chemical and Biomolecular Engineering, Department of Materials Science and Engineering, University of Pennsylvania, Philadelphia, Pennsylvania 19104, United States.

#### Notes

The authors declare no competing financial interest.

## **ACKNOWLEDGMENTS**

We thank the University of Maryland College Park for funding. We thank the Analytical NMR Research & Service Center at the University of Maryland, College Park for providing NMR services. We acknowledge Dr. Yue Li and the Mass Spec Facility in the Department of Chemistry and Biochemistry at the University of

Maryland-College Park for the use of JEOl AccuTOF mass spectrometer. We acknowledge the support of the Maryland NanoCenter and its AIM Lab. We gratefully acknowledge the support of the Center for Integrated Nanotechnologies, an Office of Science User Facility operated by the US DOE Office of Science. Sandia National Laboratories is a multimission laboratory managed and operated by National Technology and Engineering Solutions of Sandia, LLC, a wholly owned subsidiary of Honeywell International, Inc., for the US DOE's National Nuclear Security Administration (contract no. DE-NA-0003525). The views expressed in the article do not necessarily represent the views of the US DOE or the US government. We acknowledge the use of facilities supported by the Laboratory for Research on the Structure of Matter and the NSF through the University of Pennsylvania Materials Research Science and Engineering Center (MRSEC) DMR-2309043. M.K.B. and K.I.W. acknowledge financial support from NSF-DMR 1904767.

# **REFERENCES**

- (1) Bolton, E. K. Chemical Industry Medal. Development of Nylon. *Ind. Eng. Chem.* **1942**, *34*, 53–58. https://doi.org/10.1021/ie50385a011.
- (2) Brehmer, B. Polyamides from Biomass Derived Monomers. In *Bio-Based Plastics: Materials and Applications*, Kabasci, S.; John Wiley & Sons, Ltd., **2013**, pp 275–293. https://doi.org/10.1002/9781118676646.ch10.
- (3) Shakiba, M.; Ghomi, E. R.; Khosravi, F.; Jouybar, S.; Bigham, A.; Zare, M.; Abdouss, M.; Moaref, R.; Ramakrishna, S. Nylon—A Material Introduction and Overview for Biomedical Applications. *Polym. Adv. Technol.* **2021**, *32*, 3368–3383. https://doi.org/10.1002/pat.5372.
- (4) Lu, Y.; Zhang, Y.; Zhang, G.; Yang, M.; Yan, S.; Shen, D. Influence of Thermal Processing on the Perfection of Crystals in Polyamide 66 and Polyamide 66/Clay Nanocomposites. *Polymer* **2004**, *45*, 8999–9009. https://doi.org/10.1016/j.polymer.2004.10.025.
- (5) Schick, C.; Androsch, R.; Schmelzer, J. W. P. Homogeneous Crystal Nucleation in Polymers. *J. Phys.: Condens. Matter* **2017**, *29*, 453002. <a href="https://doi.org/10.1088/1361-648x/aa7fe0">https://doi.org/10.1088/1361-648x/aa7fe0</a>.
- (6) Li, Y.; Goddard, W. A. Nylon 6 Crystal Structures, Folds, and Lamellae from Theory. *Macromolecules* **2002**, *35*, 8440–8455. https://doi.org/10.1021/ma020815n.
- (7) Feldman, A. Y.; Wachtel, E.; Vaughan, G. B. M.; Weinberg, A.; Marom, G. The Brill Transition in Transcrystalline Nylon-66. *Macromolecules* **2006**, *39*, 4455–4459. https://doi.org/10.1021/ma060487h.
- (8) Starkweather, H. W.; Whitney, J. F.; Johnson, D. R. Crystalline Order in Nylon 66. *J. Polym. Sci., Part A: Gen. Pap.* **1963**, *1*, 715–723. https://doi.org/10.1002/pol.1963.100010211.
- (9) Jackson, C. L.; Shaw, M. T. Polymer Liquid Crystalline Materials. *Int. Mater. Rev.* **1991**, *36*, 165–186. https://doi.org/10.1179/imr.1991.36.1.165.

- (10) Schadt, R. J.; Gardner, K. H.; Gabara, V.; Allen, S. R.; English, A. D.; Chase, D. B. Dynamic Structure of Poly(p-Phenyleneterephthalamide). *Macromolecules* **1993**, *26*, 6509–6516. https://doi.org/10.1021/ma00076a031.
- (11) García, J. M.; García, F. C.; Serna, F.; Peña, J. L. de la. High-Performance Aromatic Polyamides. *Prog. Polym. Sci.* **2010**, *35*, 623–686. <a href="https://doi.org/10.1016/j.progpolymsci.2009.09.002">https://doi.org/10.1016/j.progpolymsci.2009.09.002</a>.
- (12) Stempfle, F.; Quinzler, D.; Heckler, I.; Mecking, S. Long-Chain Linear C19 and C23 Monomers and Polycondensates from Unsaturated Fatty Acid Esters. *Macromolecules* **2011**, *44*, 4159–4166. https://doi.org/10.1021/ma200627e.
- (13) Atallah, P.; Wagener, K. B.; Schulz, M. D. ADMET: The Future Revealed. *Macromolecules* **2013**, *46*, 4735–4741. https://doi.org/10.1021/ma400067b.
- (14) Park, J.; Staiger, A.; Mecking, S.; Winey, K. I. Ordered Nanostructures in Thin Films of Precise Ion-Containing Multiblock Copolymers. *ACS Cent. Sci.* **2022**, *8*, 388–393. <a href="https://doi.org/10.1021/acscentsci.1c01594">https://doi.org/10.1021/acscentsci.1c01594</a>.
- (15) Aitken, B. S.; Buitrago, C. F.; Heffley, J. D.; Lee, M.; Gibson, H. W.; Winey, K. I.; Wagener, K. B. Precision Ionomers: Synthesis and Thermal/Mechanical Characterization. *Macromolecules* **2012**, *45*, 681–687. <a href="https://doi.org/10.1021/ma202304s">https://doi.org/10.1021/ma202304s</a>.
- (16) Yan, L.; Rank, C.; Mecking, S.; Winey, K. I. Gyroid and Other Ordered Morphologies in Single-Ion Conducting Polymers and Their Impact on Ion Conductivity. *J. Am. Chem. Soc.* **2020**, *142*, 857–866. https://doi.org/10.1021/jacs.9b09701.
- (17) Park, J.; Staiger, A.; Mecking, S.; Winey, K. I. Enhanced Li-Ion Transport through Selectively Solvated Ionic Layers of Single-Ion Conducting Multiblock Copolymers. *ACS Macro Lett.* **2022**, *11*, 1008–1013. <a href="https://doi.org/10.1021/acsmacrolett.2c00288">https://doi.org/10.1021/acsmacrolett.2c00288</a>.
- (18) Park, J.; Winey, K. I. Double Gyroid Morphologies in Precise Ion-Containing Multiblock Copolymers Synthesized via Step-Growth Polymerization. *JACS Au* **2022**, *2*, 1769–1780. <a href="https://doi.org/10.1021/jacsau.2c00254">https://doi.org/10.1021/jacsau.2c00254</a>.
- (19) Park, J.; Easterling, C. P.; Armstrong, C. C.; Huber, D. L.; Bowman, J. I.; Sumerlin, B. S.; Winey, K. I.; Taylor, M. K. Nanoscale Layers of Precise Ion-Containing Polyamides with Lithiated Phenyl Sulfonate in the Polymer Backbone. *Polym. Chem.* **2022**, *13*, 5811–5819. <a href="https://doi.org/10.1039/d2py00802e">https://doi.org/10.1039/d2py00802e</a>.
- (20) Piroux, F.; Espuche, E.; Mercier, R.; Pinéri, M. Water Vapour Transport Mechanism in Naphthalenic Sulfonated Polyimides. *J. Membr. Sci.* **2003**, *223*, 127–139. <a href="https://doi.org/10.1016/s0376-7388(03)00315-6">https://doi.org/10.1016/s0376-7388(03)00315-6</a>.
- (21) Tricoli, V.; Carretta, N. Polymer Electrolyte Membranes Formed of Sulfonated Polyethylene. *Electrochem. Commun.* **2002**, 4, 272–276. https://doi.org/10.1016/s1388-2481(02)00269-2.
- (22) Long, L.; Wang, S.; Xiao, M.; Meng, Y. Polymer Electrolytes for Lithium Polymer Batteries. *J. Mater. Chem. A.* **2016**, *4*, 10038–10069. https://doi.org/10.1039/c6ta02621d.

- (23) Rajagopalan, P.; Kim, J.; Brack, H. P.; Lu, X.; Eisenberg, A.; Weiss, R. A.; Risen, W. M. Molecular Interpretation of Miscibility in Polyamide-6 Blends with Alkali Ionomers of Sulfonated Polystyrene. *J. Polym. Sci. Part B: Polym. Phys.* **1995**, *33*, 495–503. https://doi.org/10.1002/polb.1995.090330318.
- (24) Molnar, A.; Eisenberg, A. Miscibility of Polyamide-6 with Lithium or Sodium Sulfonated Polystyrene Ionomers. *Macromolecules* **1992**, *25*, 5774–5782. <a href="https://doi.org/10.1021/ma00047a032">https://doi.org/10.1021/ma00047a032</a>.
- (25) Molnár, A.; Eisenberg, A. Miscibility of Carboxylated and Sulfonated Polystyrene Ionomers with Polyamides-66, -610 and -11. *Polymer* **1993**, *34*, 1918–1924. <a href="https://doi.org/10.1016/0032-3861(93)90436-e">https://doi.org/10.1016/0032-3861(93)90436-e</a>.
- (26) Liu, Y.; Cui, L.; Guan, F.; Gao, Y.; Hedin, N. E.; Zhu, L.; Fong, H. Crystalline Morphology and Polymorphic Phase Transitions in Electrospun Nylon-6 Nanofibers. *Macromolecules* **2007**, *40*, 6283–6290. <a href="https://doi.org/10.1021/ma070039p">https://doi.org/10.1021/ma070039p</a>.

# Insert Table of Contents artwork here

